

Temperature Field Analysis of Mine Flameproof Outer Rotor Permanent Magnet Synchronous Motor with Different Cooling Schemes

Shengnan Wu, *Member IEEE*, Daquan Hao, and Wenming Tong, *Member, IEEE*

Abstract—Aiming at the problem of temperature rise of mine flameproof outer rotor permanent magnet synchronous motor, based on the fluid structure coupling method, the temperature distribution of motor under three cooling schemes of air cooling and water cooling are calculated respectively. For the structure I air cooling system, the influence of different number of heat sink on the maximum temperature rise and pressure drop of fluid channel is analyzed, and the parameters of heat sink are optimized. For the structure II air cooling system, the influence of setting fillet at the turn back of the fluid channel on the head loss in the fluid domain of the motor is analyzed, and the influence of different fillet radius on the head loss and the maximum temperature rise in the fluid domain is obtained. For the structure II water cooling system, the influence of different water flow speed on the maximum temperature rise of the motor is analyzed, and the influence of different assembly clearance of modular stator teeth and yoke on the maximum temperature rise of the motor is analyzed. The cooling effect and temperature rise distribution characteristics of the three cooling schemes are compared and analyzed. Finally, a water-cooled prototype is manufactured, and the temperature rise experiment is carried out, and the influence of the thermal deformation of fluid channel, stator yoke and stator teeth on the maximum temperature of the motor is analyzed. The results show that the calculated temperature field after considering the thermal deformation is closer to the experimental value, which verifies the accuracy of the calculation results, It also provides a reference for the selection and design of the cooling structure of the same type of PMSM electric roller.

Index Terms—Permanent magnet synchronous motor with outer rotor, Fluid structure coupling, Maximum temperature rise and head loss, Assembly clearance and thermal deformation.

Manuscript received June 09, 2021; revised September 11, 2021; accepted January 12, 2022. date of publication June 25, 2022; date of current version June 18, 2022.

This work has been supported by the National Natural Science Foundation of China (51907129); Project Supported by Department of Science and Technology of Liaoning Province (2021-MS-236).

Shengnan Wu is with the School of Electrical Engineering, Shenyang University of Technology, Shenyang 110870, China (e-mail: imwushengnan@163.com).

Daquan Hao is with the School of Electrical Engineering, Shenyang University of Technology, Shenyang 110870, China(e-mail:dq201920269@163.com).

Wenming Tong is with the National Engineering Research Center for Rare Earth Permanent Magnet Machines, Shenyang University of Technology, Shenyang 110870, China (e-mail: twm822@126.com).

(Corresponding Author: Wenming Tong)

Digital Object Identifier 10.30941/CESTEMS.2022.00022

I. INTRODUCTION

THIS mine flameproof outer rotor permanent magnet synchronous electric roller is the further development of permanent magnet direct drive system. It integrates the outer rotor permanent magnet synchronous motor with the driving roller, realizes the electromechanical integration, and has the advantages of convenient installation and small space occupation. With the further development of the industrial motor, the temperature rise of the motor has become an important factor restricting the continuous improvement of the single machine capacity and torque density of the motor. Therefore, it is very important to select and design the reasonable heat dissipation system of the motor and analyze the temperature field and fluid field.

At present, the common methods for calculating and analyzing the temperature field and fluid field at home and abroad include the path algorithm of equivalent thermal network or equivalent fluid network and the field algorithm based on finite volume and computational fluid dynamics (CFD) [1]-[5]. In reference [6], the CFD method is used to compare the spiral, axial Z-shaped and radial Z-shaped cooling channels for vehicle permanent magnet synchronous motor (PMSM) from the aspects of flow velocity, pressure difference and temperature rise. In reference [7], the three-dimensional transient temperature field of PMSM for external rotor crane with special working system was calculated by finite element method. In reference [8], the equivalent thermal network temperature field analysis model and three-dimensional finite element model of hub motor are established, and the steady-state temperature field distribution and transient temperature rise curve of hub motor under rated condition are calculated. In reference [9], the equivalent fluid network method was used to calculate the fluid field of a permanent magnet direct drive motor. In reference [10], a high-speed permanent magnet synchronous motor was studied based on the three-dimensional finite element method and the coupling theory of electromagnetic field, flow field and temperature field. In reference [15], the thermal calculation of a water-cooled high power density permanent magnet synchronous motor is carried out by using the equivalent thermal network and fluid structure coupling method. In reference [16], the temperature distribution of high-speed permanent magnet synchronous motor under four cooling modes is calculated by using the

magnetothermal coupling method, and the temperature field distribution under four cooling schemes is obtained. In reference [17], a modeling and thermal analysis method combining analytical and finite element is proposed for air-cooled traction motor. This method saves computing time, but it needs to write a separate code to connect and couple the analysis and finite element model, so this modeling and analysis method is more complex. In reference [18], the internal ventilation area of high-voltage motor is divided into four equal pressure areas by field circuit coupling method, and the temperature field and fluid field of the motor are analyzed. In reference [19], a multi physical field simulation method based on magneto thermal fluid coupling iterative solution is proposed, the thermal analysis of high-speed permanent magnet synchronous motor with magnetic bearing is carried out, but the influence of eddy current loss of permanent magnet is ignored. In reference [20], the magnetic heat flow coupling method is used to carry out the thermal analysis of an outer rotor cooled by spiral water channel and the synchronous motor, but there is a lack of experiments to verify the accuracy of the calculation results.

At home and abroad, the research on the temperature field and cooling of the motor is mainly concentrated in wind power generation, new energy electric vehicles and other industrial fields. There are few reports on the temperature field and cooling of the mine flameproof permanent magnet synchronous motor drum at home and abroad. In this paper, two kinds of cooling structures are proposed for the flameproof permanent magnet synchronous motor drum by CFD method, and the influence of different cooling structures and different cooling media on the temperature field of the motor is analyzed. Then the prototype of the water cooling system with the best cooling effect is manufactured and the temperature rise experiment is carried out, which verifies the accuracy of the CFD calculation results. It provides a reference for the selection and design of the cooling structure of the same type of permanent magnet synchronous electric roller.

II. MOTOR MODEL

A. Physical Model

The PMSM structure of flameproof out rotor studied in this paper is shown in Fig. 1, and the specific parameters are shown in Table I. Permanent magnet adopts surface attached structure. The permanent magnet synchronous electric drum shaft is stationary when working, the outer rotor rotates, the drum is directly connected with the load, which saves the low-speed coupling, and has the characteristics of small space occupation and convenient installation and construction.

B. Cooling Structure

According to the structure characteristics and heat source distribution, the cooling structure of the mine flameproof out rotor PMSM is set inside the stator yoke. The inner side of the stator yoke of the cooling structure I is provided with heat dissipation fins, which are arrayed along the circumference to form a heat dissipation device. The cooling air is driven by an external independent fan, flows through the inner side of the

stator yoke, absorbs the heat generated by the motor, and then is discharged through the air outlet. The cooling structure I model is shown in Fig. 2. In the cooling structure II, an axial Z-shaped fluid channel is arranged on the inner side of the stator yoke, the inlet and outlet of the fluid channel are arranged on the stationary shaft, and the inlet and outlet of the fluid channel of the stationary shaft are respectively connected with the axial Z-shaped fluid channel on the inner side of the stator yoke. The cooling medium flows in from the inlet on the stationary shaft and absorbs the heat generated by the motor through the Z-shaped fluid channel arranged on the inner side of the stator yoke, From the outlet on the stationary shaft, the structural cooling system model is shown in Fig. 3.



Fig. 1. Mine flameproof PMSM.

TABLE I
MOTOR PARAMETERS

Parameter	Value	Parameter	Value
Rated power P/kW	125	rotor diameter D_2/mm	800
Rated speed n/rpm	75	stator diameter D_{11}/mm	748
Pole pairs p	25	air gap δ/mm	1.5
Stator slots Q	60	axial length L_{ef}/mm	650

The influence of cooling structure I air cooling, cooling structure II air cooling and cooling structure II water cooling on the temperature field of the motor is studied in this paper.

III. SOLUTION OF TEMPERATURE FIELD AND FLUID FIELD

A. Basic Assumptions and Boundary Conditions

In order to reduce the difficulty of meshing, it is necessary to simplify the solution domain model to simplify the parts which have little influence on the heat transfer of the motor. In addition, in addition to copper wire, there are winding paint film, impregnating paint, inter layer insulation and slot insulation in stator slot. The filling material is complex, so the following assumptions need to be made[11],[12]:

- 1) The motor is in good impregnation condition and the impregnation paint is filled evenly.
- 2) The insulating paint of copper wire is evenly distributed.
- 3) Ignore the temperature difference between strands due to the existence of insulating paint film.
- 4) It is considered that the heating condition of the windings

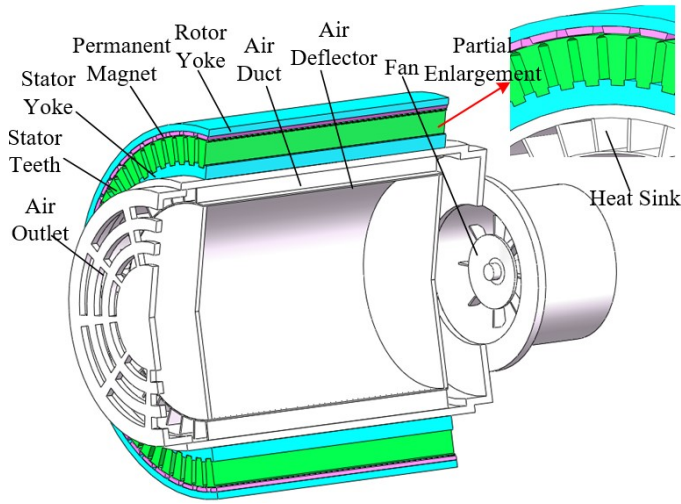


Fig. 2. Structure I cooling system model.

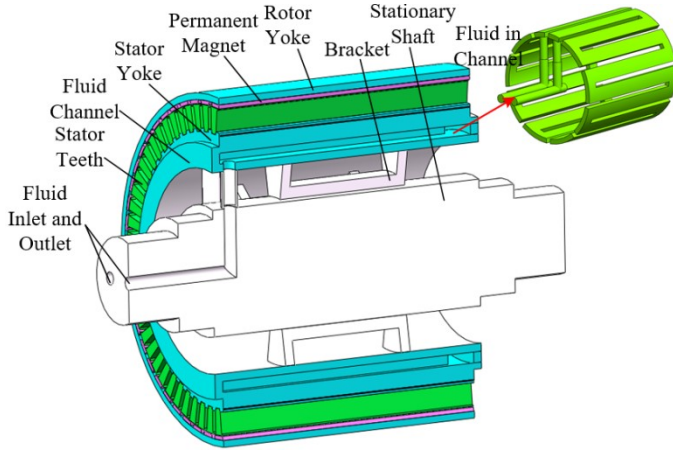


Fig. 3. Structure II cooling system model.

in the stator slot is the same, and the skin effect of the windings is ignored.

5) The radiation heat transfer is neglected.

The end winding is simplified. The end winding is equivalent to the linear type. The length of the end winding is calculated according to the following formula:

$$l_1 = \frac{1}{2} \times \left(\frac{1}{2} l_w - l_{ef} \right) \quad (1)$$

Where l_1 , l_w , l_{ef} are the length of winding end, winding full turn and core respectively. The boundary conditions are as follows:

1) The ambient temperature of the three cooling schemes is set to 300 K.

2) The air cooling duct inlet of cooling structure I is set as velocity inlet, the inlet velocity is 10 m/s, and the pressure outlet is a standard atmospheric pressure.

3) The air cooling inlet of cooling structure II is velocity inlet, the inlet velocity is 13.1 m/s, and the pressure outlet is a standard atmospheric pressure.

4) The water cooling inlet of cooling structure II is velocity inlet, the inlet velocity is 1 m/s, and the pressure type outlet is a standard atmospheric pressure.

5) Considering the influence of rotor rotation on heat transfer, the contact surface between the outer rotor and the air gap is set as the rotating wall, and the rotating speed is the rated speed.

6) The natural convection heat dissipation coefficient is 10 W/(m·K) at the end of winding and 14 W/(m·K) at the outer surface of outer rotor yoke.

B. Calculation of Equivalent Thermal Conductivity

Slot insulation, winding insulation, interlayer insulation and impregnating varnish are equivalent to an insulating entity. The thermal conductivity of equivalent insulation in stator slot can be calculated according to the following formula[13]:

$$\lambda_{eq} = \sum_{i=1}^n \delta_i / \left(\sum_{i=1}^n \delta_i / \lambda_i \right) \quad (2)$$

Where, λ_{eq} is the thermal conductivity of equivalent insulation; δ_i is the equivalent thickness of each insulating material; λ_i is the average thermal conductivity of each insulating material. The thermal conductivity of motor components is shown in Table II.

TABLE II
THERMAL CONDUCTIVITY OF EACH MATERIAL OF MOTOR

Parts	Thermal Conductivity/(W/m/K)		
	X Direction	Y Direction	Z Direction
Stator and rotor core	39	39	4.43
Air	0.0305	0.0305	0.0305
Copper	385	385	385
Permanent magnet	9	9	9
Winding insulation	0.19	0.19	0.19
Slot wedge	0.21	0.21	0.21

C. Heat Source

In this paper, the loss of mine flameproof outer rotor PMSM can be divided into stator iron loss, armature winding copper loss and stray loss. It is assumed that the stray loss is evenly distributed on the permanent magnet and stator teeth, and the friction loss generated during the operation of the motor is ignored. The loss and heat generation rate of each part of the motor under rated operation are shown in Table III.

IV. ANALYSIS OF THE RESULTS OF FLUID FIELD AND TEMPERATURE FIELD

The stator teeth and yoke of the outer rotor PMSM studied in this paper are modular spliced together, as shown in Fig. 4. After assembly, there will be a certain assembly clearance. The size of assembly clearance will have a great influence on heat transfer. Therefore, the effect of assembly clearance on heat transfer must be considered. The assembly clearance is mainly affected by the processing technology. Considering the influence of processing technology on assembly, the clearance between stator teeth and stator yoke is 0.14 mm.

TABLE III
LOSS AND HEAT GENERATION RATE UNDER RATED OPERATION

Parts	Winding	Stator Tooth	Stator Yoke	Permanent Magnet
loss/W	6107.3	2505.7	158.7	312.5
heat generation rate/(W/m ²)	364943.3	46013.4	4845.3	30796.0

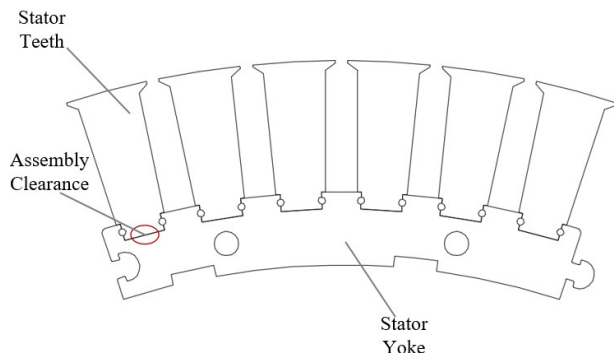


Fig. 4. Modular stator teeth and yoke.

A. Cooling Structure I air Cooling

According to the symmetry of the cooling system in the circumferential direction, the one fifth solution domain model of the motor and its cooling system is established, as shown in Fig. 5 (a). The fluid structure coupling calculation is carried out, and the temperature distribution of the permanent magnet and winding after optimizing the heat sink is shown in Fig. 6. It can be seen from Fig. 6 that the highest temperature rise in the solution domain is located at the end of the winding, which is 62.0 K, and the overall temperature distribution is uneven along the axial direction. Starting from the air inlet side, the overall temperature gradually rises, with the maximum temperature difference at both ends of the winding of 19.9 K and the maximum temperature difference at both ends of the permanent magnet of 3.2 K.

The influence of different number of heat sink on the maximum temperature rise of the motor is shown in Fig. 7 below. It can be seen from the Fig. 7 that when the inlet velocity remains unchanged, the maximum temperature rise of the motor decreases with the increase of the number of cooling ribs, and the decreasing trend gradually slows down. When the number of heat sink is 40, 60, 80, 100 and 120, that is, the heat dissipation area is doubled every time, the maximum temperature rise of the motor decreases by 11.5 K, 7.3 K, 5.6 K, 4.1 K and 2.8 K respectively. When the number of ribs is 115, the heat dissipation area increases by 4.75 times, and the maximum temperature rise decreases by 31.5%; When the number of heat sink is 130, the heat dissipation area increases by 5.5 times, and the maximum temperature rise of the motor is 0.7 K lower than that of 120. However, as the number of heat sink increases, the flow resistance of fluid through the duct increases, and the pressure drop in the duct increases. The influence of the number of heat sink on the fluid pressure drop in the air duct is shown in Fig. 8. It can be seen from the figure that when the number of cooling ribs increases from 20 to 130, the fluid pressure drop in the air duct increases by 314%.

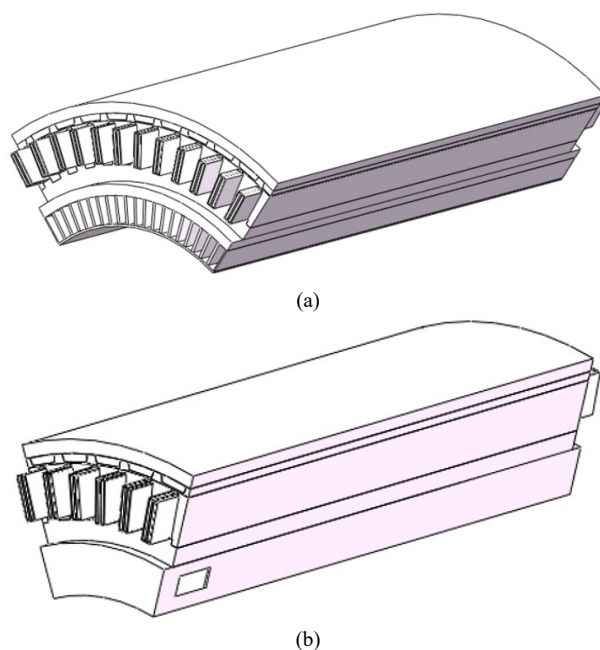


Fig. 5. Fluid structure coupling model of cooling structure I and cooling structure II. (a) cooling structure I. (b) cooling structure II.

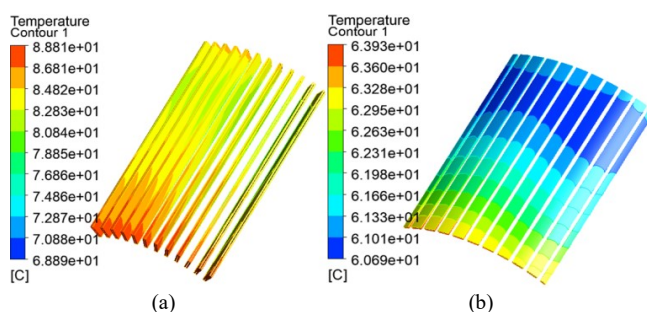


Fig. 6. Temperature distribution of armature winding and permanent magnet. (a) armature winding. (b) permanent magnet.

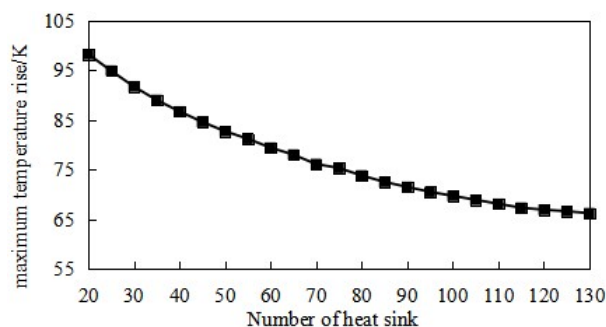


Fig. 7. Influence of different number of heat ribs on maximum temperature rise of motor.

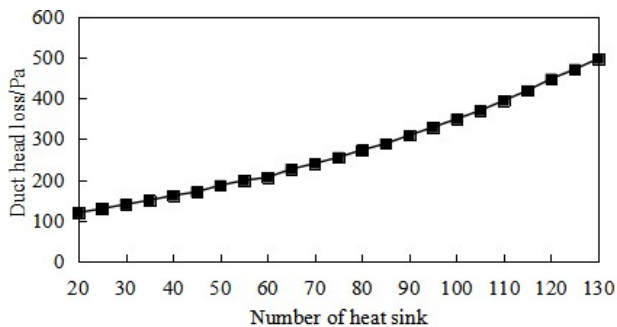


Fig. 8. Influence of different number of ribs on pressure drop in air duct.

Table IV shows the influence of different sizes of heat sink on the maximum temperature rise of the motor when the number of heat sink is 115. It can be seen from table IV that keeping the height of heat sink unchanged, when the thickness of heat sink increases from 1mm to 7 mm, the maximum temperature rise of the motor first decreases and then increases. When the thickness of heat sink is 4 mm, the maximum temperature rise of the motor is the lowest. The reason is that when the width of the heat sink is small, the radial heat transfer area of the heat sink is small, resulting in large heat transfer resistance, and the temperature rise of the motor decreases with the increase of the width of the heat sink; When the width of the heat sink exceeds the critical value of 4 mm, increasing the width of the heat sink will reduce the contact area between the solid and the fluid in the fluid channel, that is, the heat sink area, and the temperature rise of the motor will increase with the increase of the width of the heat sink. When the height of the ribs increases from 20 mm to 65 mm, the maximum temperature rise of the motor decreases by 20.8 K, and the decreasing trend of the maximum temperature rise gradually slows down with the increase of the height of the heat sink.

TABLE IV
INFLUENCE OF DIFFERENT SIZE OF HEAT SINK ON MAXIMUM TEMPERATURE RISE OF MOTOR

Size (Width×Height) / (mm×mm)	Maximum temperature rise/K	Size (Width×Height) / (mm×mm)	Maximum temperature rise/K
1×40	70.2	4×25	77.0
2×40	68.2	4×30	73.2
3×40	67.8	4×35	70.6
4×40	67.7	4×45	66.4
5×40	68.7	4×50	64.9
6×40	69.5	4×55	63.5
7×40	71.2	4×60	62.8
4×20	82.8	4×65	62.0

B. Cooling Structure II Air Cooling

The internal fluid channel structure of cooling structure II is an axial Z-shaped channel. The width of two fluid channels is taken as the solution domain model [14]. The fluid in the fluid channel can be air or water. The solution domain model of cooling structure II is shown in Fig. 5 (b). Firstly, the situation that the fluid in the flow passage is air is analyzed, and the temperature distribution of armature winding and permanent magnet is shown in Fig. 9.

It can be seen from the figure that the highest temperature rise in the solution domain is located at both ends of the winding, which is 98.3 K. The temperature rise distribution of the winding shows that the temperature rise of the upper is higher than that of the lower end, and the maximum temperature difference is 15.6 K. The temperature of the whole solution region is lower in the middle, and the temperature rises to both ends in turn. This is because the heat of winding is

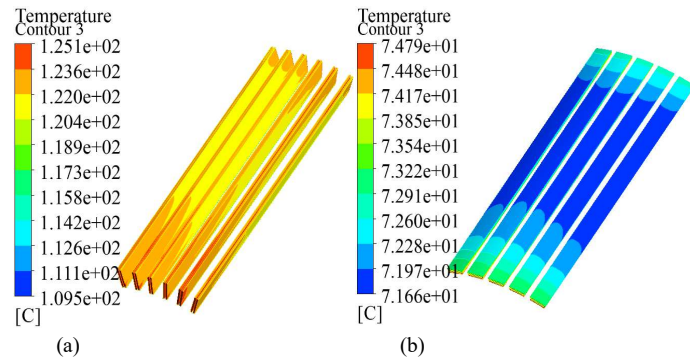


Fig. 9. Temperature distribution of armature winding and permanent magnet. (a) armature winding. (b) permanent magnet.

mainly transferred to the fluid channel along the radial direction through heat conduction. The heat transfer resistance of winding near the fluid channel is low and the heat transfer is relatively high.

In cooling structure II, when the fluid turns back many times, there will be a large fluid pressure drop, so the fan needs to increase the power to provide enough air pressure. In order to reduce the burden of the fan, the fillet is set at the corner of the fluid channel to reduce the flow resistance, as shown in Fig. 10. The influence of different fillet radius on the head loss of fluid channel is shown in Fig. 11, and the influence of different fillet radius on the maximum temperature rise of motor is shown in Fig. 12.

It can be seen from Fig. 11 that the flow resistance of the flow channel can be significantly reduced by setting a fillet at the corner of the flow channel, thus reducing the pressure head loss of the fan. With the increase of fillet radius, the head loss of fan decreases gradually, and the decreasing trend becomes gentle. When the fillet radius reaches 12 mm, the head loss of fan decreases by 49.4%. It can be seen from Fig. 12 that the maximum temperature rise of the motor increases with the increase of the fillet radius. With the increase of the fillet radius by 2 mm, the maximum temperature rise of the motor increases by 0.5-1.6K. This is because the flow velocity at the bend of the flow channel after rounding, that is, the inner side of the bend of the Z-shaped flow channel, decreases, which affects the maximum temperature of the motor.

C. Cooling Structure II Water Cooling

When the fluid in the channel is water, the inlet velocity is 1m/s, the hydraulic diameter is 33.6 mm. The temperature distribution of armature winding and permanent magnet is shown in Fig. 13. It can be seen from the figure that the highest temperature rise in the solution domain is located at the end of the winding, which is 46.0 K, the highest temperature difference of the winding is 18.2 K, the highest temperature rise of the permanent magnet is 21.6 K, and the highest temperature difference is 1.7 K. On the whole, the temperature in the middle is relatively low, and the temperature at both ends is relatively high.

The influence of different water velocity on the maximum temperature rise of the motor is shown in Fig. 14. It can be seen from the figure that with the increase of water velocity, the

maximum temperature rise of the motor gradually decreases, and the downward trend gradually slows down. When the water velocity increases from 0.1 m/s to 1 m/s, the maximum temperature rise of the motor decreases by 6.2 K, and the maximum temperature rise decreases by 11.9%; When the water velocity increases from 1m/s to 1.5 m/s, the maximum temperature rise of the motor decreases by 0.4 K, and the maximum temperature rise decreases by 0.9%.

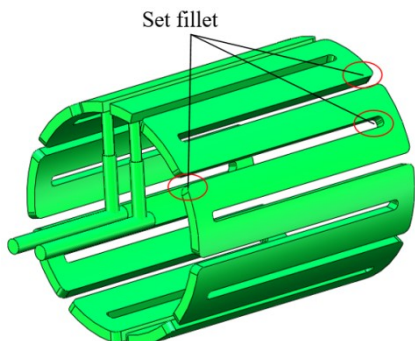


Fig. 10. Cooling structure II channel fluid.

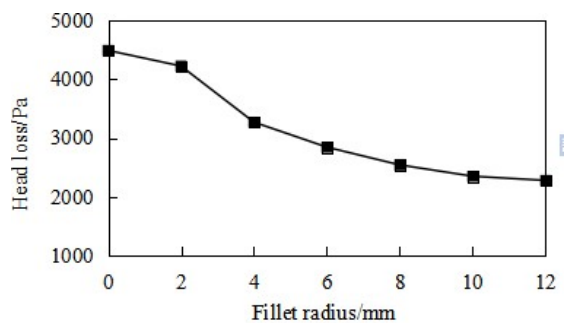


Fig. 11. Influence of different fillet radius on fluid head loss in channel.

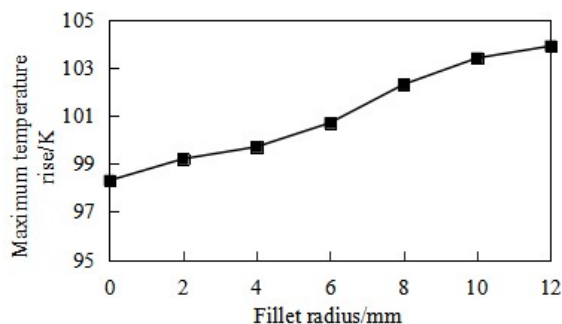


Fig. 12. Influence of different fillet radius on maximum temperature rise of motor.

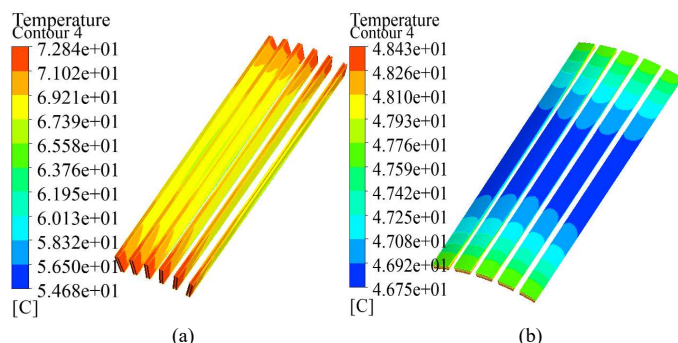


Fig. 13. Temperature distribution of armature winding and permanent magnet. (a) armature winding. (b) permanent magnet.

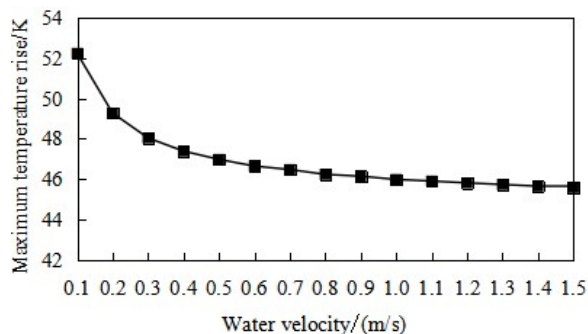


Fig. 14. Influence of different water velocity on maximum temperature rise.

The influence of different assembly clearance between stator teeth and stator yoke on the maximum temperature rise of the motor is shown in Fig. 15. It can be seen from the figure that the maximum temperature rise of the motor increases with the increase of the assembly clearance between stator teeth and stator yoke. When the assembly clearance increases by 0.05 mm, the maximum temperature rise of the motor increases by 5-8 K.

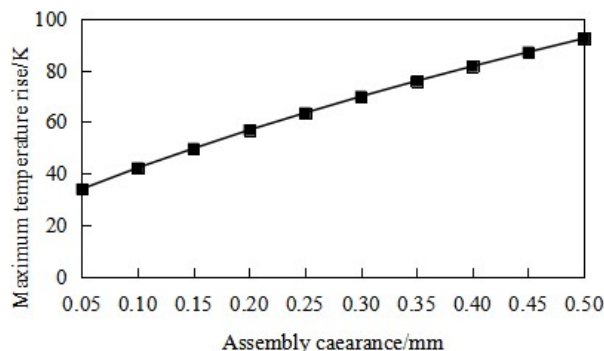


Fig. 15. Influence of different assembly clearance on maximum temperature rise.

V. COMPARATIVE ANALYSIS

The temperature of parts of the motor under the three cooling schemes is shown in Table V below. It can be seen from the table that the cooling effect of cooling structure II water cooling scheme is the best, and the maximum temperature rise of winding is 46.0 K, but the water cooling system is more complex; The second is cooling structure I air cooling. The maximum temperature rise of winding is 62.0 K, which has good cooling effect, but independent fan is required to drive cooling air; Cooling structure II air cooling scheme has the worst cooling effect, the maximum temperature rise of winding is 98.3 K, the cooling effect is poor and the cooling structure is complex. In the three cooling schemes, the highest temperature is located in the winding, followed by the stator teeth, because the heat source of the stator teeth is the largest except the winding. On the other hand, there is insulation with small thermal conductivity between the stator winding and the stator teeth, and the thermal resistance between the stator winding and the stator teeth is large, which limits the heat transfer between the winding and the stator teeth.

TABLE V
MAXIMUM TEMPERATURE RISE OF PARTS UNDER THREE COOLING SCHEMES

Part	Winding/ K	Stator Teeth/K	Stator Yoke/K	Permanent Magnet/K
Structure I air cooling	62.0	56.1	25.4	37.1
structure II air cooling	98.3	90.7	66.0	48.0
Structure II water cooling	46.0	40.3	7.4	21.6

VI. EXPERIMENTAL VERIFICATION

In order to verify the accuracy of the finite volume method to calculate the temperature rise of the motor, the structure II water cooling temperature rise experimental platform is built for the temperature rise experiment, as shown in Fig. 16. The measured outer rotor permanent magnet synchronous electric drum is connected with the load through the belt. The temperature sensor is embedded in the inner winding of the measured outer rotor permanent magnet synchronous electric drum to measure the winding temperature, and the temperature of the outer rotor yoke is measured by the infrared thermometer.

Because of the temperature difference between the fluid channel and stator yoke, between stator yoke and stator teeth, the effect of assembly tolerance caused by thermal deformation on the heat transfer of motor is considered in order to make the calculation results more accurate. The assembly tolerance caused by thermal deformation between fluid channel and stator yoke, stator yoke and stator tooth is analyzed by coupling fluent module and static module in ANSYS software. The assembly tolerance caused by thermal deformation between fluid channel and stator yoke is 0.019 mm, and the assembly tolerance caused by thermal deformation between stator yoke and stator tooth is 0.015 mm. The calculated and experimental values of temperature of each component after considering the assembly tolerance caused by thermal deformation are shown in Table VI. Among them, the calculation value I is the assembly tolerance caused by the thermal deformation is not considered, and the calculation value II is the assembly tolerance caused by the thermal deformation. It can be seen from the table that the calculation results of each component after considering the assembly tolerance caused by thermal deformation are close to the experimental values, among which the error of calculated value of winding temperature rise is reduced from 7.4% to 3.2%, and the calculated error of rotor yoke temperature rise is reduced from 3.1% to 1.3%. The results of the calculation are in good agreement with the temperature rise experiment, and the error is within the acceptable range, which proves the accuracy of the calculation results.

VII. CONCLUSION

In this paper, the fluid structure coupling numerical method is used to calculate and analyze the temperature of mine flameproof outer rotor PMSM under three cooling schemes of air cooling and water cooling, and the influence of three cooling schemes on the maximum temperature rise of the motor is compared. The following conclusions can be drawn:



Fig. 16. Temperature rise experiment platform.

TABLE VI
COMPARISON OF CALCULATED AND EXPERIMENTAL VALUES OF MOTOR
TEMPERATURE RISE

Parts	Experimental Value/K	Calculated Value I/K	Error I/%	Calculated Value II/K	Error II/%
Winding	49.7	46.0	7.4	48.1	3.2
Rotor yoke	22.3	21.6	3.1	22.0	1.3

1) The maximum temperature difference between the two ends of the winding is 19.9 K, and the maximum temperature rise of the motor is 62.0 K after the optimization of the heat sink for the air cooling system of cooling structure I; The results show that the overall temperature rise distribution of air cooling and water cooling of cooling structure II is low in the middle and high at both ends; The air cooling effect of cooling structure II is poor. The maximum temperature rise of motor is 98.3 K and the maximum temperature difference of winding is 15.6 K; The maximum temperature rise of cooling structure II water-cooled motor is 46.0 K, and the maximum temperature difference of winding is 18.2 K.

2) For the air cooling system of cooling structure I, the maximum temperature rise decreases by 31.5% when the heat dissipation area of the heat sink increases by 4.75 times, and then the influence of the heat dissipation area on the maximum temperature rise of the motor is small. The pressure drop in the duct increases with the number of heat sink; The maximum temperature rise first decreases and then increases with the increase of the heat sink width, that is, there is an optimal width; The maximum temperature rise decreases with the increase of the heat sink height, and the decreasing trend gradually slows down.

3) For the cooling structure II air cooling system, when the fillet radius increases from 0 mm to 12 mm, the head loss of the fan decreases by 49.4%. For the cooling structure II water-cooling system, when the water velocity increases from 0.1 m/s to 1 m/s, the maximum temperature rise of the motor decreases by 11.9%, and when the water velocity increases from 1 m/s to 1.5 m/s, the maximum temperature rise of the motor decreases by 0.9%. When the assembly clearance between stator teeth and stator yoke increases by 0.05 mm, the maximum temperature rise of the motor increases by 5-8 K.

4) Considering the assembly tolerance caused by the thermal deformation between the fluid passage and stator yoke, and between the stator yoke and stator teeth, the temperature rise

calculation results are closer to the experimental values, in which the error of winding temperature rise calculation value is reduced from 7.4% to 3.2%, and the error of rotor yoke temperature rise calculation value is reduced from 3.1% to 1.3%.

REFERENCES

- [1] X Y Wang, C Zhou, "Thermal Analysis and Cooling Approach Design of Axial Flux Permanent Magnet Synchronous Machines With PCB Winding" *Proceedings of the CSEE*, vol. 36, no, 11, pp. 3062-3069, Nov, 2016.
- [2] W M Tong, X B Cheng, S L Shu, "Calculation and analysis of fluid field and temperature field for high-speed permanent magnet motor" , *Advanced Technology of Electrical Engineering an Energy*, vol. 35, no, 5, pp. 23-28, May, 2016.
- [3] Sciascera C, Giangrande P, Papini L, et al, "Analytical Thermal Model for Fast Stator Winding Temperature Prediction", *IEEE Transactions on Industrial Electronics*, vol. 64, no, 8, pp:6116-6126, Aug, 2017.
- [4] Nachousne B A, Abdelli A, Friedrich G, et al, "Numerical approach for thermal analysis of heat transfer into a very narrow air gap of a totally enclosed permanent magnet integrated starter generator" in *Proc. of IEEE Energy Conversion Congress and Exposition*, Montreal Canada, 2015, pp. 1749-1756.
- [5] Boglietti A, Cavagnino A, Lazzari M, et al, "A simplified thermal model for variable-speed self-cooled industrial induction motor", *IEEE Transactions on Industry Applications*, vol. 39, no, 4, pp. 945-952, July-Aug, 2003.
- [6] X F Wang, Y Dai, J Luo, "Waterway Design and Temperature Field Analysis of Vehicle Permanent Magnet Synchronous Motor Based on Fluid-Solid Coupling", *Transactions of China Electrotechnical Society*, vol. 34, no, 1, pp. 22-29, June, 2019.
- [7] X Y Han, K Qi, Q L Duan, "Numerical calculation and analysis of 3D transient temperature field in the exterior-rotor PMSM for crane", *Electric Machines & Control*, vol. 19, no, 5, pp. 44-52, May, 2015.
- [8] X Y Wang, P Gao, "Application of Equivalent Thermal Network Method and Finite Element Method in Temperature Calculation of in-Wheel Motor", *Transactions of China Electrotechnical Sociey*, vol. 31, no, 16, pp. 26-33, Aug, 2016.
- [9] W M Tong, S N Wu, R Y Tang, "Totally enclosed self circulation axial ventilation system design and thermal analysis of a 1.65MW direct drive PMSM", *IEEE transactions on industrial electronics*, vol. 65, no, 12, pp:9388-9398, Dec, 2018.
- [10] Y Chen, J Zhou, Y Fang, et al, "Multi-field coupling finite-element analysis of the temperature rise in permanent magnet synchronous motor applied for high speed train", *IEEE International Conference on Electrical Machines and Systems*, Chiba Japan, 2016, pp. 1-4.
- [11] Habibinia D, Rostaami N, Feyzi M R, et al, "New finite element based method for thermal analysis of axial flux interior rotor permanent magnet synchronous machine", *IET Electric Power Applications*, vol. 14, no, 3, pp.464-470, Dec, 2020.
- [12] Boglietti A, Cossalem M, Popescu M, et al, "Electrical Machines Thermal Model: Advanced Calibration Techniques", *IEEE Transactions on Industry Applications*, vol. 55, no, 3, pp.2620-2628, May-June, 2019.
- [13] Ilhan E, Kremers M F J, Motoasca T E, et al, "Transient thermal analysis of flux switching PM machines" in *Proc. of International Conference and Exhibition on Ecological Vehicles and Renewable Energies*, Monte Carlo, 2013, pp. 1-7.
- [14] W L Li, S F Li, Ying Xie, et al, "Stator rotor Coupled Thermal Field Numerical Calculation of Induction Motors and Correlated Factors Sensitivity Analysis", *Proceedings of the CSEE*, vol. 24, no, 3, pp. 85-91, Aug, 2007.
- [15] Y Xu, B Zhang and G. Feng, "Research on Thermal Capacity of a High-Torque-Density Direct Drive Permanent Magnet Synchronous Machine Based on a Temperature Cycling Module," *IEEE Access*, vol. 8, pp. 155721-155731, Aug, 2020.
- [16] G Du, W Xu, J Zhu, et al, "Power Loss and Thermal Analysis for High-Power High-Speed Permanent Magnet Machines," *IEEE Transactions on Industrial Electronics*, vol. 67, no. 4, pp. 2722-2733, April, 2020.
- [17] S Nategh, H Zhang, O Wallmark, et al, "Transient Thermal Modeling and Analysis of Railway Traction Motors," *IEEE Transactions on Industrial Electronics*, vol. 66, no. 1, pp. 79-89, Jan. 2019.
- [18] M Ai, Y Yang, Y Xu, et al, "Research on Thermal Characteristics of Internal Ventilated Paths in Compact Medium High- Voltage Motor Based Fluid Network Decoupling," *IEEE Access*, vol. 7, pp. 79268-79276, Jun, 2019.
- [19] B Dong, K Wang, B Han, et al, "Thermal Analysis and Experimental Validation of a 30 kW 60000 r/min High-Speed Permanent Magnet Motor With Magnetic Bearings," *IEEE Access*, vol. 7, pp. 92184-92192, July, 2019.
- [20] Q Chen, H Shao, J Huang, et al, "Analysis of Temperature Field and Water Cooling of Outer Rotor In-Wheel Motor for Electric Vehicle," *IEEE Access*, vol. 7, pp. 140142-140151, Sep, 2019.



Shengnan Wu (M'18) was born in Yingkou, China. She received the B.S., M.S., and Ph.D. degrees in electrical engineering from the Shenyang University of Technology, Shenyang, China, in 2008, 2011, and 2017, respectively.

She is currently a Postdoctoral Research Assistant in electrical engineering with Shenyang University of Technology. Her research interests include electromagnetic design and multiphysical field simulation and analysis of permanent magnet machines.



Daquan Hao was born in Liaoning, China. He received the B.S. degree in electrical engineering from Liaoning Shihau University, Fushun, China, in 2019. He is currently working toward the M.S. degree in electrical engineering with the Shenyang University of Technology, Shenyang, China. His main research interests include multiphysical field simulation and analysis of permanent magnet machines.



Wenming Tong (M'18) was born in Dandong, China. He received the B.S. and Ph.D. degrees in electrical engineering from the Shenyang University of Technology, Shenyang, China, in 2007 and 2012, respectively.

He is currently an Associate Professor with the National Engineering Research Center for Rare Earth Permanent Magnet Machines, Shenyang University of Technology. His major research interests include the design, analysis, and control of high-speed and low-speed direct drive permanent magnet machines, axial flux permanent magnet machines, hybrid excitation machines, and high-performance machines with new types of soft magnetic materials.